Water Resources Research

RESEARCH ARTICLE
10.1029/2023WR036626

Special Collection:
Hydrogeodesy: Understanding changes in water resources using space geodetic observations

Interferometric Radar Satellite and In-Situ Well Time-Series Reveal Groundwater Extraction Rate Changes in Urban and Rural Afghanistan

N. Kakar[1], S. Metzger[1], T. Schöne[1], M. Motagh[1,2], H. Waizy[3], N. A. Nasrat[3], M. Lazecký[4,5], F. Amelung[6], and B. Bookhagen[7]

[1]GFZ Helmholtz Centre for Geosciences, Potsdam, Germany, [2]Institute of Photogrammetry and GeoInformation, Leibniz University Hannover, Hannover, Germany, [3]Faculty of Geology and Mines, Kabul Polytechnic University (KPU), Kabul, Afghanistan, [4]COMET, School of Earth and Environment, University of Leeds, Leeds, UK, [5]IT4Innovations, VSB-TU Ostrava, Ostrava-Poruba, Czechia, [6]Department of Marine Geosciences, Rosenstiel School of Marine, Atmospheric, and Earth Science, University of Miami, Coral Gables, FL, USA, [7]University of Potsdam (UP), Potsdam-Golm, Germany

Key Points:

- Afghan-wide subsidence data highlights several urban and agricultural centers with more than 7 mm/yr of subsidence between 2015 and 2022
- Droughts and increased groundwater pumping caused subsidence of 31.2 cm in Kabul over ~6 and 77.8 cm in Ghazni over ~7 years
- In farmlands, mapped solar panels serve as a proxy for groundwater extraction and acceleration of subsidence using electrical pumps

Supporting Information:

Supporting Information may be found in the online version of this article.

Correspondence to:

N. Kakar,
najibullah.kakar@gfz.de

Citation:

Kakar, N., Metzger, S., Schöne, T., Motagh, M., Waizy, H., Nasrat, N. A., et al. (2025). Interferometric radar satellite and in-situ well time-series reveal groundwater extraction rate changes in urban and rural Afghanistan. *Water Resources Research*, *61*, e2023WR036626. https://doi.org/10.1029/2023WR036626

Received 13 MAR 2024
Accepted 12 FEB 2025

Author Contribution:

Conceptualization: N. Kakar
Data curation: N. Kakar
Formal analysis: N. Kakar
Investigation: N. Kakar
Methodology: N. Kakar
Resources: N. Kakar
Software: N. Kakar
Validation: N. Kakar
Visualization: N. Kakar

Abstract

Population growth, climate change, and a lack of infrastructure have contributed to an increase in water demand and groundwater exploitation in urban and rural Afghanistan, resulting in significant ground subsidence. Based on a 7-year-long Sentinel-1 radar-interferometric time-series (2015–2022), we assess country-wide subsidence rates. Of particular focus are urban Kabul and the growing agricultural sector of rural Ghazni. In Kabul, we compare spatiotemporal subsidence patterns to water table heights and precipitation amounts. In Ghazni, we monitored the transition from ancient to modern irrigation techniques by mapping solar-panel arrays as a proxy for electrical water pumping and evaluating the vegetation index as a proxy for agricultural activity. Several cultural centers (Kabul, Ghazni, Helmand, Farah, Baghlan, and Kunduz) exhibit significant subsidence of more than ~5 ± 0.1 cm/yr. In Kabul, ground subsidence is largest near the city center with a 6-year total of 31.2 ± 0.5 cm, but the peripheral wells of the Kabul basin exhibit the highest water-table drops. In Ghazni, with a 7-year total of 77.8 ± 0.5 cm, subsidence rates are dramatically accelerating since 2018. Before 2018, barren land was transformed into farmland and traditional irrigation was replaced by electrical water pumps to tap groundwater. As a result, m-wide and km-long desiccation cracks appeared in the area with the highest irrigation volume and subsidence.

Plain Language Summary

Political instability in Afghanistan limited access to freshwater resources for decades. At the same time, population growth, climate change, and more efficient electric water pumps lead to an increased demand for this vital resource. As a consequence, the lowering water table causes severe land subsidence in several Afghan cities and agricultural centers. Using space-borne radar measurements from 2015 to 2022, we mapped Afghan land subsidence and found about 31 cm of subsidence over 6 years in Kabul city and about 78 cm over 7 years in the Ghazni agricultural province. In Kabul, we measured the fastest subsidence near the city center, but it is the wells in the marginal districts that are affected the most because here, the aquifers are thinnest and thus most vulnerable. In Ghazni, the land subsidence is caused by turning barren into fertile land and by excessive electrical pumping of groundwater since 2016 for farming. The subsidence problem was intensified by droughts in 2020 and 2021 that caused meter-wide surface cracks over a length of a few kilometers in 2022.

1. Introduction

The past and ongoing social and political unrest in Afghanistan caused significant infrastructure damage. The destruction of irrigation and water-supply systems severely impacted farming and water-resource management. The recent conflicts prevented an efficient surface-water management using dams or canals, thus, groundwater is one of the main freshwater sources (Mack et al., 2013; Meldebekova et al., 2020). In addition, resettlement between urban and rural regions exacerbates water scarcity (Green et al., 2011) and forces the communities to exploit additional groundwater sources. Technical advances such as solar panels and water pumps have boosted groundwater use for civil, agriculture, and industrial purposes, but water scarcity persists. In Kabul, the (estimated) annual groundwater use of 30×10^6 to 40×10^6 m^3/yr appears to outrun the annual groundwater recharge during wet periods (15×10^6 to 40×10^6 m^3/yr) already for quite some time (Houben et al., 2009). In rural regions, ancient subterranean well networks, called Qanat or Kariz, collected annual ground water from elevated foothills

Writing – original draft: N. Kakar
Writing – review & editing: N. Kakar

and transported it to the farm lands. They formed a sustainable system for many generations (Ebrahimi et al., 2021), but their efficiency is now reduced by ongoing climate change (Shokory et al., 2023). Increasing water demand and temperatures, seasonally shifting precipitation, and reduced contributions from the cryosphere all lead to unsustainable groundwater use (NEPA & UN Environment, 2016). We hypothesize that this must reflect in severe ground subsidence in areas with unconsolidated geologic units across the whole country. The bordering state of Iran faces similar climatic and socio-cultural conditions, and the full extent of the dramatic subsidence has only recently been discovered (e.g., Haghshenas Haghighi & Motagh, 2024). First attempts to map recent subsidence in Afghanistan reported 5.3 cm/yr subsidence for Kabul (Meldebekova et al., 2020), but a countrywide assessment is still missing.

Regional subsidence caused by groundwater extraction in densely-populated areas has been reported worldwide. By 2040, 19% of the global population might be affected, causing costs of more than 8 trillion USD (Fernández-Torres et al., 2020; Herrera-García et al., 2021). Subsidence is often observed near large, governmental-controlled pumps such as in Mexico City (10–50 cm/yr, Chaussard et al., 2021), the Iranian Mashad Valley (20 cm/yr, Motagh et al., 2007), Jakarta (6 cm/yr, Bott et al., 2021), or the Californian San Joaquin Valley (4.2 cm/yr, with peak subsidence of 34 cm in 2016, Neely et al., 2021). In Afghanistan, however, privately-owned, small pumps dominate, which might affect aquifers differently. To better understand and assess Afghan groundwater use and its surface response, we need to quantify extraction rates and link them to the local social, seasonal, and climatic conditions.

Ground-based observation techniques like accurate positioning (GNSS, e.g., Ikehara, 1994), spirit leveling (Bitelli, 1991), or airborne Light Detection and Ranging (LiDAR, Froese & Shilong, 2008) provide pointwise information and/or are expensive and currently inapplicable to Afghan subsidence studies. Open-access gravity measurements from the GRACE-FO satellite mission (Boergens et al., 2022; Flechtner et al., 2016; Long et al., 2016) monitor the Earth's water cycle in a resolution that is spatially too low (∼300 km) to monitor local and countrywide ground subsidence. Better-suited are satellite radar interferometric (InSAR) data remotely collected by the European Copernicus Sentinel-1 mission that build time-series with high spatiotemporal resolution (tens of meters, 12/24 days of revisit time) (Torres et al., 2012).

A single radar interferogram measures ground displacement as a function of the (ambiguous) phase change along the satellite's line-of-sight (LOS) with cm accuracy (Massonnet & Feigl, 1998). InSAR works best in a dry atmosphere as it is biased by atmospheric and ionospheric delays but also by soil-moisture changes (Ansari et al., 2021). It is challenging to apply InSAR in regions with dense vegetation or snow coverage due to temporal decorrelation. To overcome these issues and improve the signal sensitivity to millimeters, the individual interferograms are combined in time-series networks that either rely on interferograms covering short observation periods only (SBAS, Berardino et al., 2002; Schmidt & Bürgmann, 2003) or on ground pixels with good backscatter-quality only (Ferretti et al., 2001). Overall, the data interpretation is rather complex and requires multiple data processing steps.

InSAR time-series have been successfully applied to quantify ground subsidence due to groundwater depletion in urban areas such as in Kabul (Meldebekova et al., 2020), Mexico city (Chaussard et al., 2021; López-Quiroz et al., 2009), Iran (Haghshenas Haghighi & Motagh, 2019, 2024), Indonesia (Siriwardane-de Zoysa et al., 2021), and as well as agricultural lands, for example, in Iran (Motagh et al., 2007, 2008), California (Ikehara, 1994; Schmidt & Bürgmann, 2003; Sneed & Brandt, 2015), and Nevada (Bell et al., 2002).

To identify all regions in Afghanistan that subside significantly due to groundwater depletion, we created countrywide surface-rate maps derived from over 7-year-long (2015–2022) InSAR time-series. We then focus in particular on two subsiding regions—Kabul city and the rural province of Ghazni—to study the spatiotemporal subsidence pattern and how it correlates to precipitation time-series and other ground-truth observations. In Kabul city, we consult well logs that monitor changes in the water table. In rural Ghazni, we compare our results to mapped desiccation cracks, ancient Kariz systems, and solar-panel arrays, as well as changes in the Normalized Difference Vegetation Index (NDVI).

2. Geologic, Geographic, and Climate Setting

The climate of Afghanistan is predominantly arid (Qutbudin et al., 2019) with the southeast being influenced by the Indian monsoon and the north by continental climate (Sarwary et al., 2022). Kabul (1,800 m asl) and Ghazni

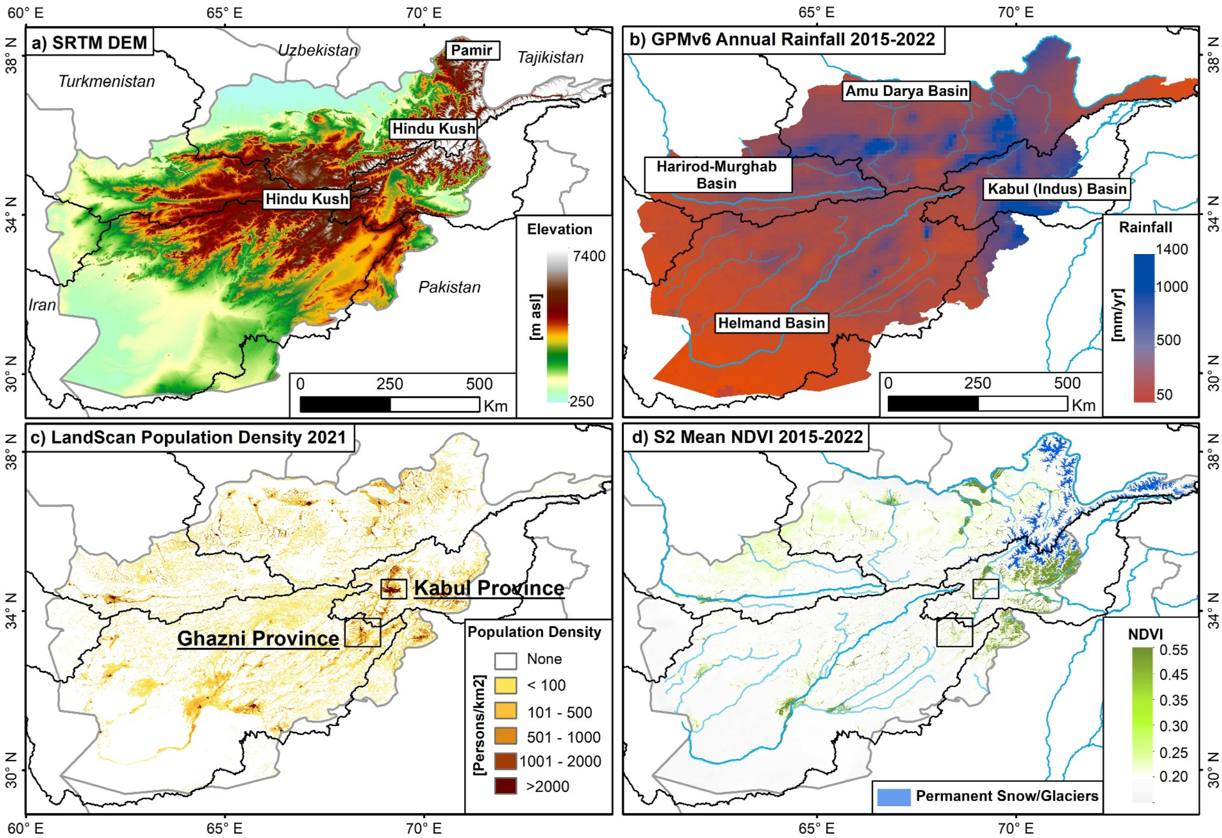

Figure 1. (a) SRTM elevation model (Farr & Kobrick, 2000), (b) satellite-derived mean annual precipitation (Huffman et al., 2023), (c) population density (Sims et al., 2021), and (d) permanent snow coverage (FAO, 2021) and mean annual Normalized Difference Vegetation Index (NDVI) from Sentinel-2 data. Black rectangles in (c) and (d) outline the study regions, blue lines in (b) and (d) show major rivers, black lines major hydrological basins, and gray lines international boundaries.

(2,200 m asl) experience cold winters, while summers can be hot and dry (Sarwary et al., 2022). Annual precipitation peaks between December and March and ceases during the summer period.

Precipitation brought by the Westerlies north of and by the Indian monsoon south of the Hindu Kush is the main source of water supply (Figures 1a and 1b). The water is distributed into the four river catchments of Amu Darya, Harirod-Murghab, Helmand, and Kabul (Indus) (Figure 1b) (Karim & Sadat, 2021) and transported to populated and agricultural regions at lower elevation (Figures 1c and 1d). In the low-relief terrain groundwater is the only all-season water source (Figure 1b) (Karim & Sadat, 2021).

The Afghan economy and food production depend on both irrigated and rainfed agriculture (Muradi & Boz, 2018). Irrigated agriculture uses river and groundwater to support multiple cropping seasons, while rainfed agriculture is currently affected by water scarcity due to climate change (Shokory et al., 2023).

Kabul is the largest urban center in Afghanistan with a population of up to 5.5 million (NSIA, National Statistic and Information Authority, 2023). It is one of the fastest-growing and water-stressed cities in the world (Hamidi et al., 2023) with plummeting groundwater levels (Meldebekova et al., 2020). Kabul is situated between prominent hills, which consist of metamorphic rocks, including Precambrian gneisses, mica slates, amphibolites, quartzites, and marbles (Homilius, 1966). The Kabul River bed consists of coarse-grained deposits with high permeability that is responsible for rapid ground-water recharge. Under Kabul city, up to 600 m of coarse sand and gravel sediments eroded from the surrounding mountains and deposited by three rivers flowing through the basin (Houben et al., 2009). The top Neogene-Quaternary layers are 30–80 m thick, thinning out toward the margins, and highly permeable with groundwater velocities of 0.2×10^{-4} to 13×10^{-4} m/s. Because of the reduced thickness of the conglomeratic layer at the basin margins, we also expect a lower subsidence response due to groundwater extraction. Toward the underlying marly basal layer, pore spaces become cemented

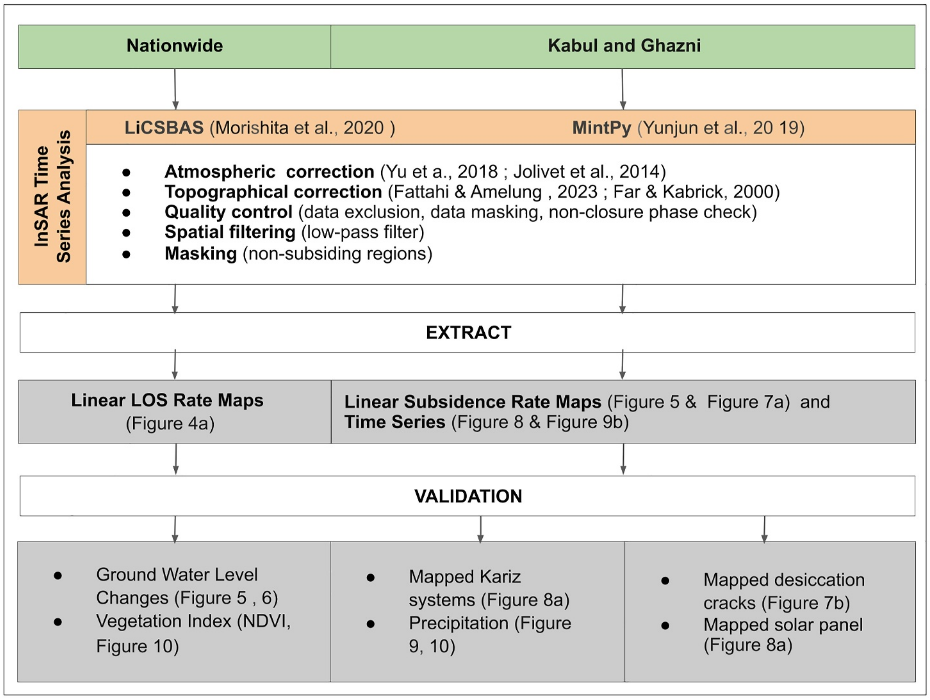

Figure 2. Flowchart of data analyses and validation for the full Afghan study (left) and the two focus areas (right). Software tools are highlighted in salmon, data products in gray.

(Houben et al., 2009). A layer of low-permeability loess covers the aquifers and acts as a protective layer (Figure S1a in Supporting Information S1) (Abdullah et al., 2008; Houben et al., 2009).

Ghazni province is located ∼150 km southwest of Kabul with an estimated population of 1.4 million (NSIA, 2023). The geological units and soil conditions are comparable to the Kabul area (Figure S1b in Supporting Information S1) (Abdullah et al., 2008). Farming is the major income, and conversion of barren to fertile lands has increased dramatically over the last years (Hekmat et al., 2023). To keep up food production with the growing population, the traditional Kariz irrigation systems have been replaced by modern irrigation practices for greenhouse farming, horticulture, and livestock (Macpherson et al., 2017).

3. Data Analysis

3.1. Methodology Overview

In a first countrywide assessment of InSAR surface rates, we identified multiple regions with significant radar range increase to the satellite. We interpret the subsidence as sediment compaction caused by significant groundwater extraction in the past decade. We focus on two study regions (Kabul and Ghazni) with a more refined time-series analysis and higher spatial resolution, and extracted vertical (subsidence) rates and pointwise subsidence time-series. In parallel, we analyzed precipitation data, digitized well water-level time-series (for Kabul only), and monitored the vegetation growth (for Ghazni only). Finally, given the lack of official information in remote Ghazni, we used optical imagery to map and monitor agricultural and environmental processes such as the geometry of the ancient Kariz irrigation networks, modern water extraction by electrical pumping, and the occurrence of desiccation cracks for the area of interest (AOI). We then integrated all observations to validate the InSAR results and study the regional subsidence processes in space and time. An overview of all analysis steps is given in Figure 1,2, while more details on each method are given below.

3.2. Interferometric Synthetic Aperture Radar (InSAR) Tme-Series Analysis

We processed Sentinel-1 imagery of 14 radar footprints (∼240 km × 200 km) in orbit-descending view geometry to build time-series and extract LOS rate maps for a first assessment of countrywide subsidence. The fully

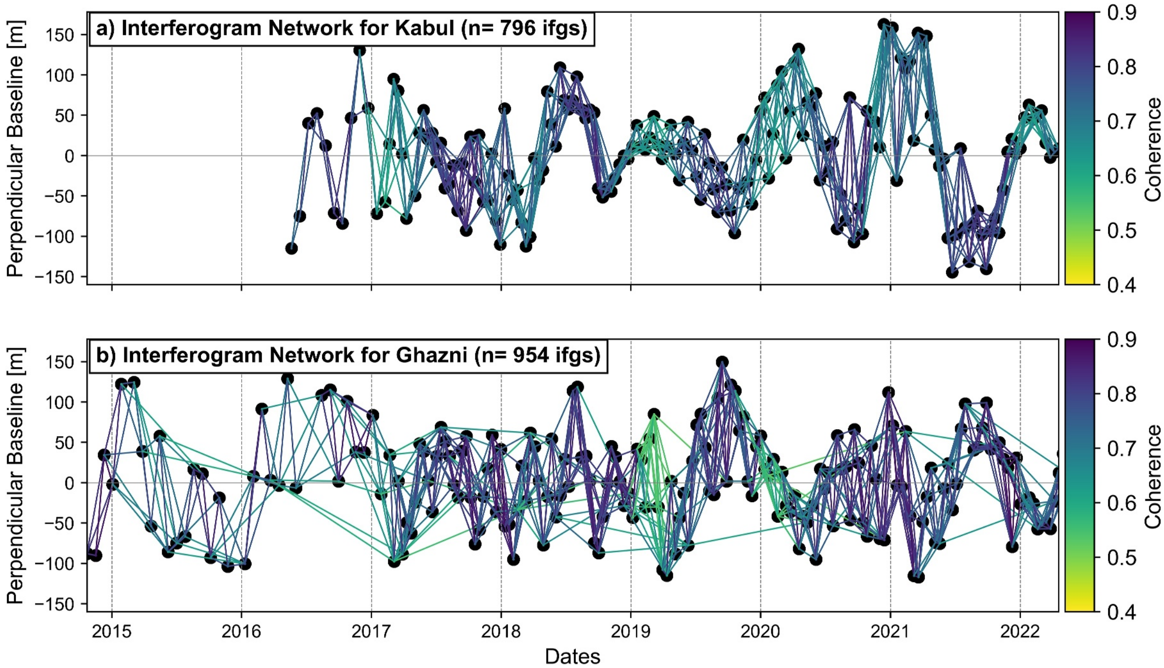

Figure 3. Interferometric networks for (a) Kabul (ascending track 71, frame 109) and (b) Ghazni (descending track 78, frame 481). Black circles mark the radar acquisitions, lines show the interferogram pairs color-coded by average coherence. The Kabul time-series starts in mid-2016 only.

automatized interferometric processing (Lazecký et al., 2020) included a downsampling (multi-looking) of the radar images by a factor of 20 along range and four along azimuth direction to ∼100 m ground resolution. The interferograms were filtered using an adaptive phase filter (Goldstein & Werner, 1998) to facilitate automatic unwrapping of the interferometric phase. Topographic phase contributions were removed using an elevation model acquired by the Shuttle Radar Topographic Mission (SRTM) (Farr & Kobrick, 2000).

We calculated displacement time-series for each footprint using the LiCSBAS software (Morishita et al., 2020) and standard parameters. To reduce computation costs, we further downsampled the input interferograms to 400 m, such that the analysis was manageable with a standard desktop computer. We subtracted the estimated atmospheric signal delay from each interferogram using weather models of the European Center for Medium-Range Weather Forecasts (ECMWF) offered by the Generic Atmospheric Correction Online Service (GACOS) (Yu et al., 2018). We excluded low-quality interferograms based on poor data coverage, low coherence (due to snow and vegetation), and phase unwrapping errors (Yunjun et al., 2019). We estimated linear rates by assuming similar displacement rates between disconnected interferometric sub-networks (López-Quiroz et al., 2009). We masked out pixels with unreliable rates based on quality markers such as temporal stability and network lengths, and we low-pass filtered the rate maps in space (2 km) and time (∼36 days). The most coherent and stable pixel was selected as reference for each frame (footprint). Finally, we flattened the rate map of each radar frame by fitting a linear plane, leaving the local subsidence pattern unchanged while minimizing the offset across the frame.

For our two study regions Kabul and Ghazni, we generated additional LOS rate maps with a spatial resolution of 40 m and a denser interferometric network. We processed 169 radar images acquired over Kabul and 192 images acquired over Ghazni using the Alaska SAR on-demand processing facility (Kennedy et al., 2021). We applied a 10×2 multi-looking and unwrapped the interferograms using Minimum Cost Flow (Chen & Zebker, 2002). The interferometric network connects each acquisition to a maximum of five preceding and successive images within 60 days (Figure 3). We also added a few 1-year-connections to reduce the impact of non-closure phase. The networks are somewhat sparser before 2017, when the repeat period was reduced from 24 to 12 days (Figure 3). The overall dry climate provides a high interferometric coherence, with lowest values of 0.5–0.6 during the rain period in winter.

We used the MintPy software (Yunjun et al., 2019) and a weighted least-square inversion for the time-series analysis. We first inverted the interferometric network with a coherence-based network modification (Perissin & Wang, 2012; Yunjun et al., 2019) using a coherence threshold of 0.7 and excluded interferograms with an area ratio (coverage) below 0.75. We performed phase-closure tests (Biggs et al., 2007; De Zan et al., 2015) to detect unwrapping errors and corrected the tropospheric signal delay using ECMWF data (Jolivet et al., 2014). We estimated the linear rates and standard deviations (Fattahi & Amelung, 2013), applied a topographical correction using a second-order polynomial function (Fattahi & Amelung, 2013), and reduced acquisition noise using the root-mean-squared residual of the estimated phase. Noisy interferograms were removed from the processing chain. The reference point of each frame was chosen by the highest average coherence (above 0.85 with the limit of 100 coherent pixels).

Soil-moisture changes on the ground may lead to a non-closure phase that significantly impacts (overestimates) the rates derived from small-baseline interferometric networks (Ansari et al., 2021). To better understand their impact, we evaluated the results of networks built by 1, 2, 3, 5, 7, and 10 interferometric connections spanning a time range from 12 days (connection 1) to 240 days (connection 10) (Maghsoudi et al., 2022; Zheng et al., 2022) and found that the minimum non-closure phase is observed in networks with 5 connections (corresponding to 60 days, see Text S2 and Figure S2 in Supporting Information S1). We also verified the impact of potential unwrapping errors by visually analyzing an interferometric chain of the year 2021 and found none (see Text S3 and Figure S3 in Supporting Information S1). For the further analysis of pointwise time-series we estimated rates by linear regression with uncertainties derived from the root-mean-square (RMS) value.

Assuming horizontal displacement to be negligible in subsiding regions (Ren & Feng, 2020), we converted the rate estimates (Figure 1) and displacement time-series from LOS to vertical by scaling them with $-1/\cos(\varphi)$, with the radar incidence angle φ ranging from 30° to 45° across the frame (Floris et al., 2019; Pepe et al., 2016). Thus, by convention, LOS subsidence is positive, representing range increase, while cosine-corrected vertical subsidence is negative.

3.3. Precipitation Data, Well Monitoring, Optical Imagery

We compare our InSAR subsidence rate maps and time-series to ground-truth data of 91 wells in Kabul logged monthly by the Afghan Ministry of Energy and Water. The well logs provide water level, pH value, water resistivity, and particle dissolution over the same period as the InSAR observations. We digitized the data logs and removed outliers visually and quantitatively. To identify a potential correlation of groundwater, water-level drop, and precipitation, we retrieved monthly precipitation data from the National Aeronautics and Space Administration (NASA) Global Precipitation Measurement (GPM v6) satellite mission (Huffman et al., 2023). In the Ghazni region, we mapped and monitored solar panel arrays (2–8 panels per array) on high-resolution optical imagery collected in 2016, 2019, and 2022 using a weighted kernel density from point features that fall within a pre-defined cell size (Silverman, 2018). The solar panel arrays serve as a proxy for family-owned wells in agricultural regions that lack well log data. We further mapped the Kariz network and m-wide desiccation cracks (Eqbal, 2022) on high-resolution (0.31 m) Maxar imagery from the WorldView-3 satellite (Maxar Technologies, 2023) and verified them in a field visit in May 2023.

4. Results

4.1. Countrywide Surface Displacement Rates

The countrywide InSAR rate maps for 2015–2022 highlight regions with significant subsidence, for example, in the Kabul urban area (~150 km^2 affected by subsidence) the highest subsidence is 6.3 ± 0.2 cm/yr between 2016 and 2019 and 3.4 ± 0.4 cm/yr between 2020 and 2022; in the agricultural region of Ghazni (~1,420 km^2) the highest is 2.6 ± 0.1 cm/yr between 2015 to mid-2018, 13.2 ± 1.1 cm/yr between mid-2018 and 2020, and 26.9 ± 0.8 cm/yr between 2021 and 2022, and in the regions around Helmand (~2,500 km^2) the highest subsidence is 6.4 ± 0.2 cm/yr from 2015 to mid-2018, and 13.9 ± 0.1 cm/yr between mid-2018 to 2022, in Farah (~1,300 km^2) the highest subsidence is 5.1 ± 0.1 cm/yr, in Baghlan (~210 km^2) the highest subsidence is 6.6 ± 0.1 cm/yr, and in Kunduz (~230 km^2) the highest subsidence is 8.9 ± 0.2 cm/yr) (Figure 4a and Figure S4 in Supporting Information S1).

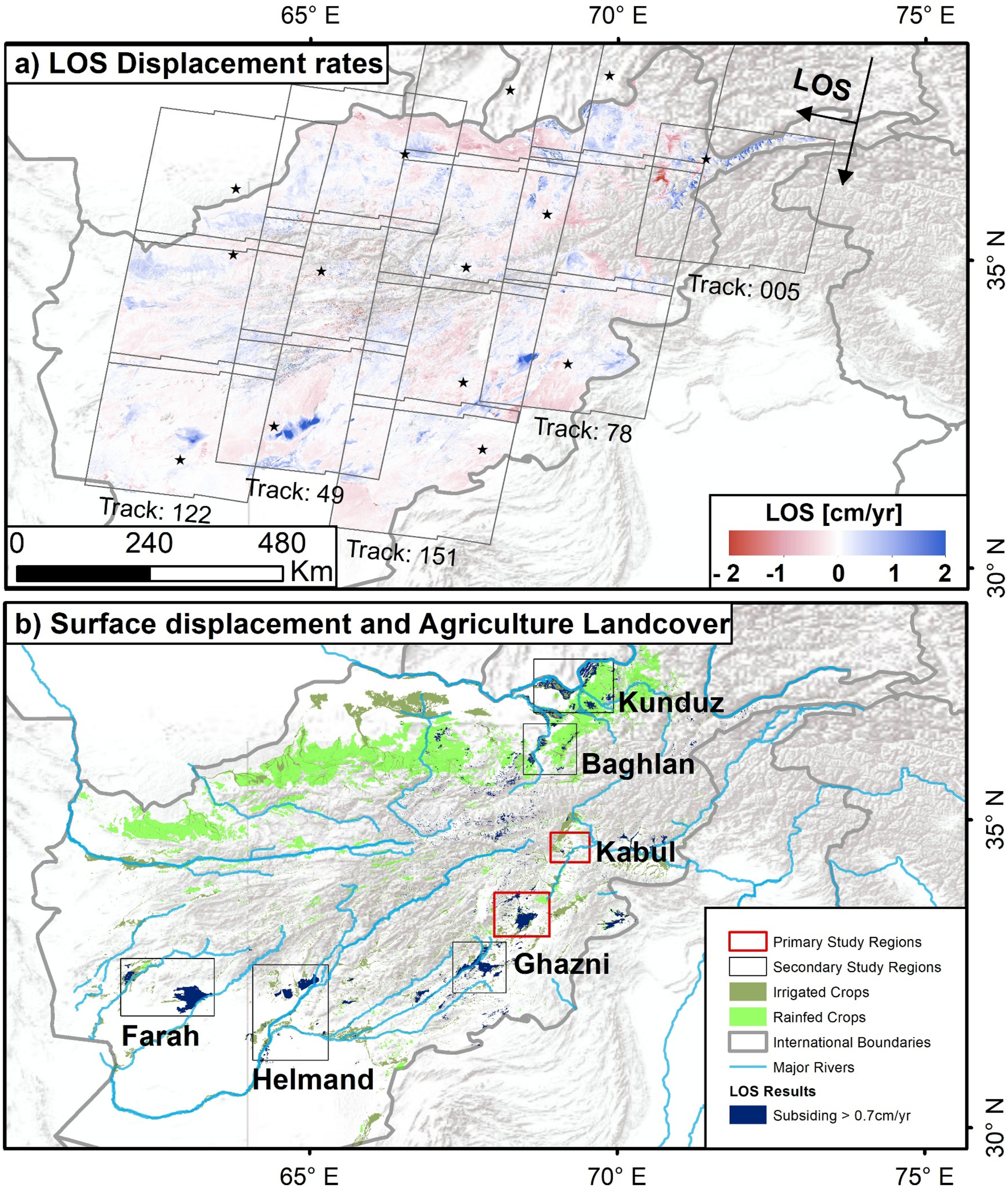

Figure 4. (a) Individual InSAR LOS rate maps of 14 Sentinel-1 acquisition frames (polygons). Positive values (in blue) represent motion away from the satellite (interpreted as subsidence), and the black stars mark the individual reference points. (b) Agricultural land use and InSAR LOS rates exceeding 0.7 cm/yr.

All these regions are either densely populated or agriculturally exploited; hence, we interpret the LOS increase as anthropogenic ground subsidence. We classified all low-elevation regions with a general LOS range increase higher than 0.7 cm/yr as subsiding (Figure 4b). We observe less subsidence in the rainfed agriculture of northern Afghanistan than in the irrigated agriculture of southern Afghanistan.

In the following, we focus on Kabul and Ghazni provinces to further investigate the observed subsidence in the country's largest city as well as in an agricultural region that—compared to the other regions—exhibits significant acceleration since 2018. We compare the high-resolution InSAR data to well-water levels, mapped solar-panel

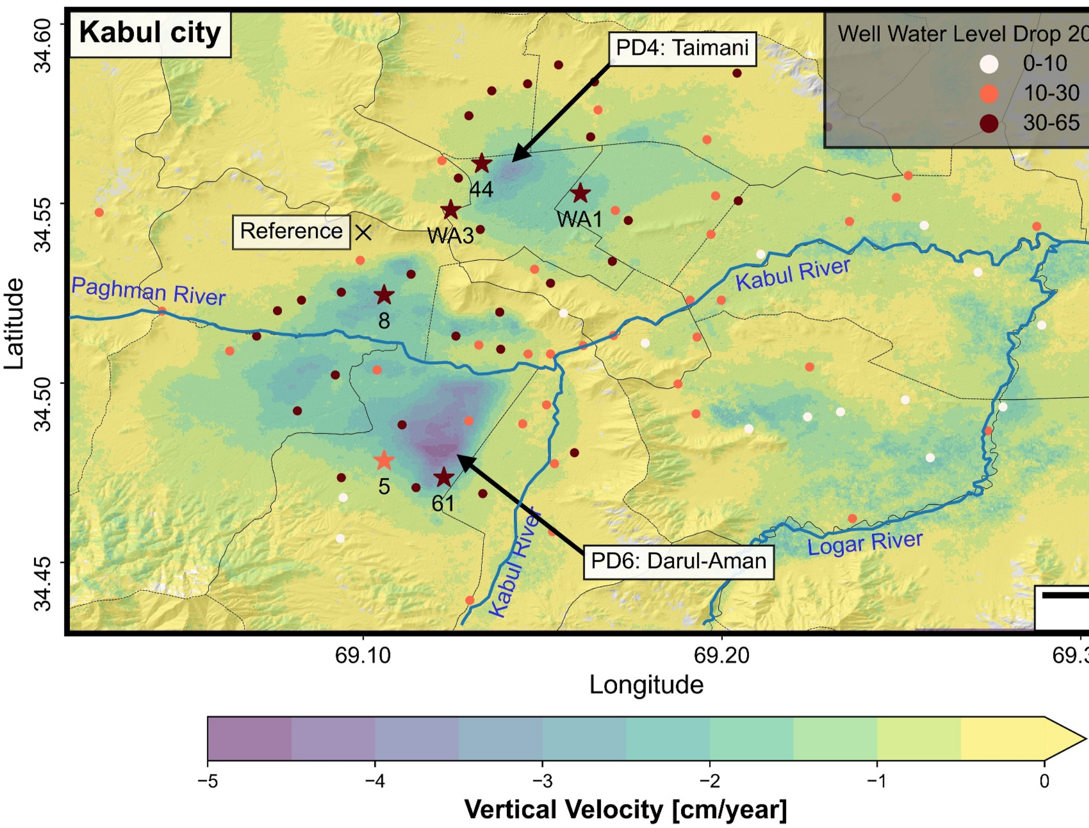

Figure 5. Averaged InSAR subsidence rates observed in Kabul city overlaid on SRTM hillshade data (cf. Figure 4b for location). Wells (circles and stars) are color-coded by the total water level drop since 2013. Stars with labels mark wells whose time-series are shown in Figure 6. Provincial districts are marked by thin lines and labeled if discussed in the text. The black cross marks the InSAR reference point.

density, Kariz systems, and recent desiccation cracks. In the discussion, we compare the InSAR data to precipitation time-series and transformational land-use activities.

4.2. Subsidence in Kabul

Kabul's northeastern and southern city centers both exhibit significant subsidence ranging from 0.5 to 5.1 ± 0.1 cm/yr (Figure 5). The area affected by subsidence correlates with the extent of the city. The strongest subsiding regions are the densely populated provincial districts Darul Aman (PD6), where most (inter-)national institutions are located and Taimani (PD4) in the north. The less populated southeastern part of the city is less affected, and the hills within and around Kabul city remain stable. Subsidence only occurs in the unconsolidated basin sediments, while the metamorphic bedrock remains unaffected (Figure S1a in Supporting Information S1). Hence, the subsidence originates from the shallow aquifers, not deep-rooted groundwater. We observe a decrease in subsidence rates from 6.3 ± 0.2 cm/yr between 2016 and 2019 to 3.4 ± 0.4 cm/yr between 2020 and 2022.

The water level in wells varies significantly across different locations (Figure 5). In peripheral Kabul, we observe a water-table drop of 30–65 m since 2013. Those wells roughly outline the spatial extent of InSAR subsidence (Figure 5). Maximum subsidence is observed in the southern city center. The water-table drop in southeastern Kabul along the Kabul River and Logar River ranges between 0 and 30 m.

Most of the well's water level time-series exhibit a quasi-linear drop (Figure 6). The water level drop in wells 5, 44, and WA1 correlates with the co-located cumulative InSAR subsidence (subfigure a, b, and c), while the water level drop in WA3 seems to be (relatively) faster (d), in well 61 and 8 slower than the InSAR observations (e, f). Thus, to first order, these data suggest that excessive extraction of groundwater leads to water table drop and ground subsidence. However, the individual wells are affected differently, because of local inhomogeneity caused

10.1029/2023WR036626

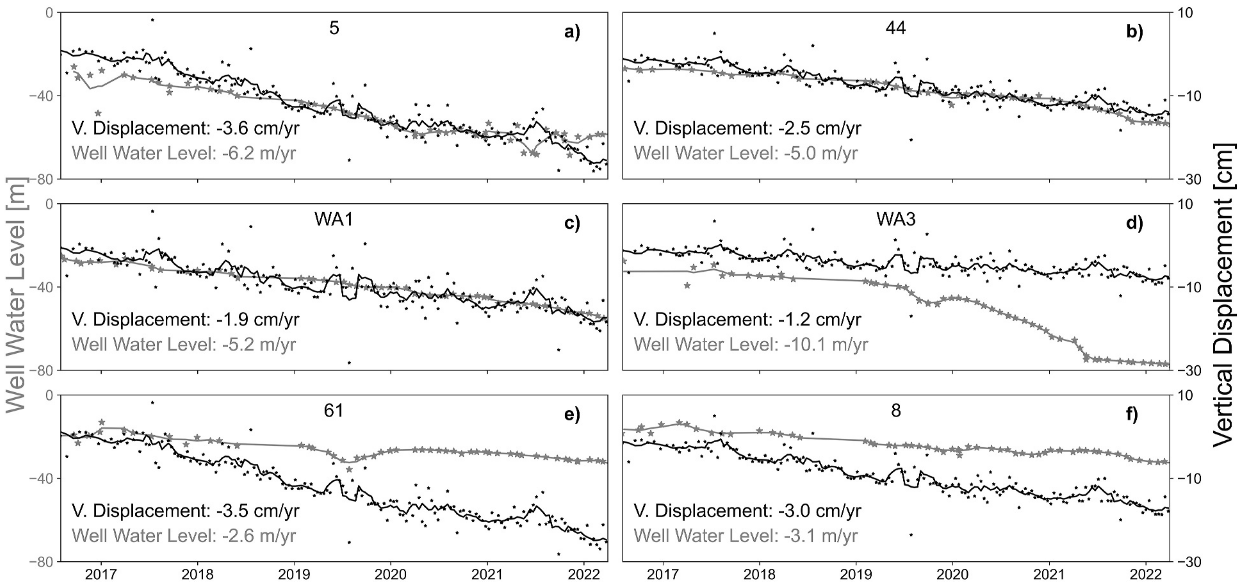

Figure 6. Water level of wells (gray) and co-located InSAR vertical displacement time-series (converted from LOS) (cf. Figure 4). The average rates derived from a linear regression are indicated in each subfigure.

by parameters like recent city development, well depth, rheological properties, sediment thickness, and aquifer extent. Shallow wells, for example, exhibit a lower water level drop (Figure 6f) than deep wells (Figures 6a and d).

4.3. Subsidence in Ghazni Agricultural Region

The agricultural lands in the southeastern part of Ghazni capital city such as Andar and Deh Yak provincial districts (Figure 7a) exhibit a total ground subsidence of 77.8 ± 0.5 cm between 2015 and 2022, leading to large tensile desiccation cracks around Deh Yak in July 2022 after two drought years (Figure 7b) (Eqbal, 2022). A field visit in August 2022 revealed cracks of up to ∼2.5 m width, 3–4 m depth, and ∼2.3 km length running parallel to the topography (or perpendicular to the slope). They roughly separate two rapidly subsiding regions located northeast and southwest of the cracks (Text S3 and Figure S3 in Supporting Information S1). Similar to the Kabul case, only the shallow sediments seem to be affected by subsidence (Figure S1b in Supporting Information S1), suggesting that the signal emanates from the shallow aquifers.

The two districts underwent significant expansion of irrigated agriculture lands in the past 10 years. The InSAR time-series exhibit increasing subsidence rates from 2.6 ± 0.1 cm/yr between 2016 and 2019 to 26.9 ± 0.8 cm/yr between 2021 and 2022 (Figure 8).

We compared InSAR subsidence rates with the number of solar panel arrays installed until 2016 (163 arrays), 2019 (1244), and 2022 (2108) (Figure 8a), documenting an increase of 660% from 2016 to 2019 and of 70% from 2019 to 2022. Density estimates using a kernel function suggest 30 arrays per km^2, and at least one deep well per hectare powered by electricity in 2022.

The area with the highest solar-panel density (labeled "NE corner" in Figure 8a) does not correlate with the highest InSAR subsidence near Deh Yak center. In the NE corner of the AOI, most of the panels were installed only after 2019 in households built on thin layers of coarse Quaternary sediments close to the mountain front and less subsidence is expected. The area with the second highest solar-power density (labeled "Deh Yak center" in Figure 8a) co-locates with heavily exploited agricultural land with more panels per array due to the relatively large size of the fields and maximum InSAR subsidence (Figure 8b). Here, the installation of solar panels already started before 2016.

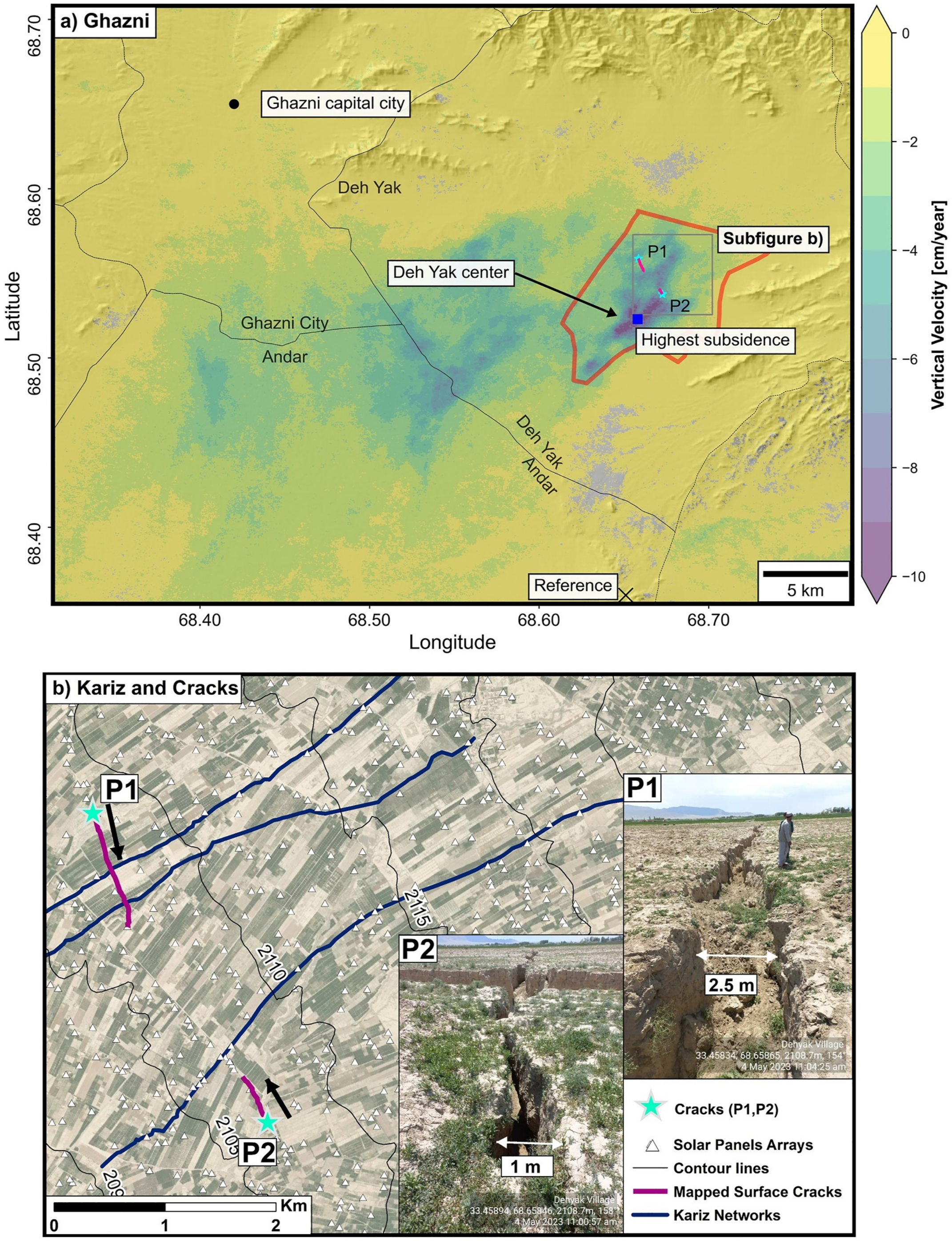

Figure 7. (a) InSAR subsidence rates around Ghazni overlaid on SRTM hillshade data (cf. Figure 4b for location). District borders in black lines, black dots are city centers, black cross marks the InSAR reference point. The red polygon outlines our study area (cf. Figure 8). (b) Solar-panel arrays (white triangles), Kariz network (thick blue lines), and elevation contours (thin black lines). Thick purple lines mark desiccation cracks confirmed in the field during August 2022, black arrows and blue stars mark the location and view angle of photographs P1 and P2.

10.1029/2023WR036626

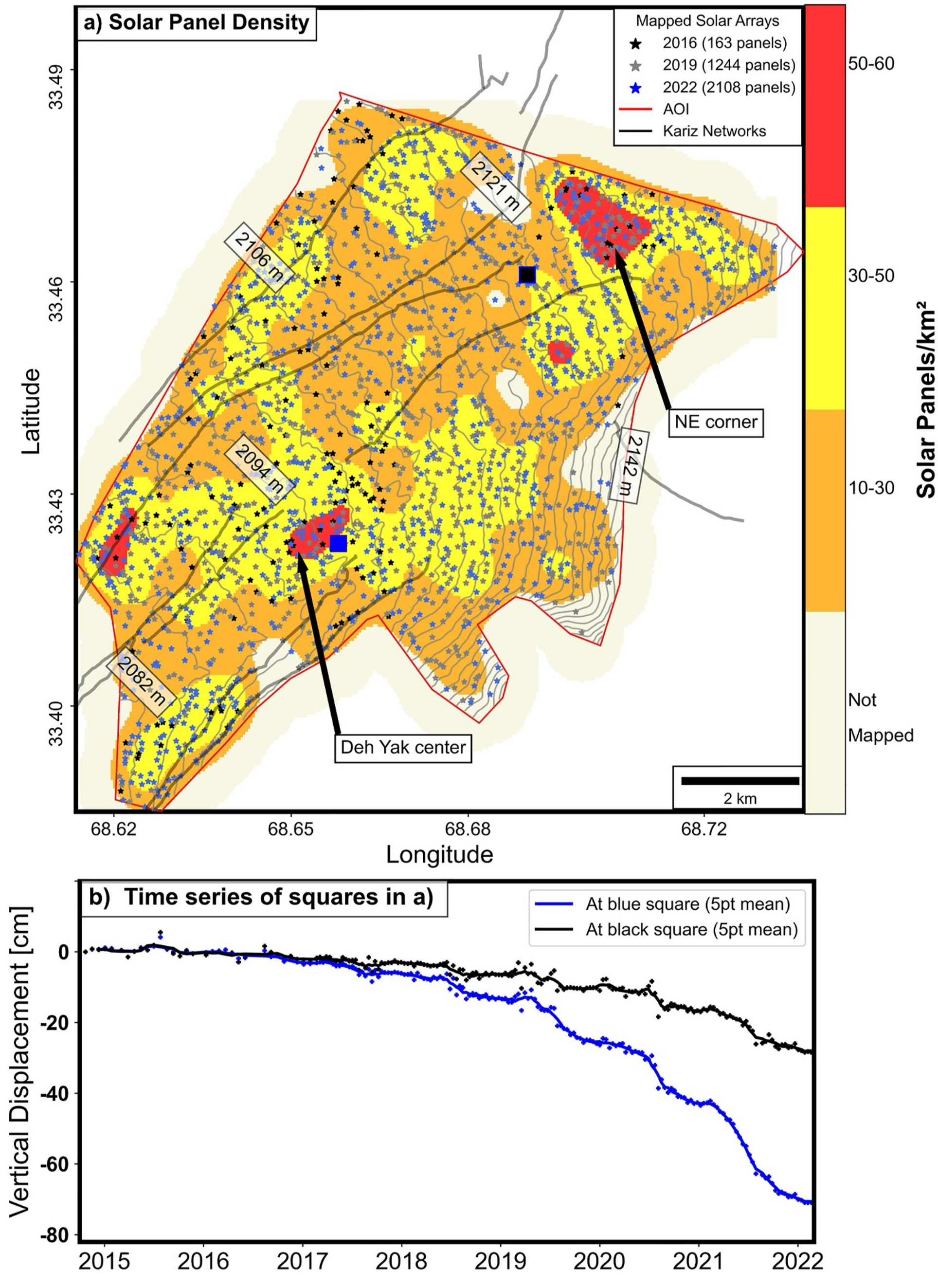

Figure 8. (a) Solar-panel density, solar panel arrays color-coded by year of appearance within our AOI, Kariz networks (black lines), and elevation contour lines (thin gray lines). (b) Characteristic examples of InSAR subsidence time-series at the blue and black square in (a). Lines average subsidence over five neighboring data points (approximately 60 days).

5. Discussion

By an improved radar-interferometric monitoring approach that includes ground validation via optical imagery, we have established a spatiotemporal correlation between ongoing ground subsidence, solar-powered pumps, and depleted groundwater resources in both rural and urban Afghan regions. The subsidence process will likely continue, even accelerate, because of population growth, climate change, and advanced technical capabilities.

Table 1
Biennial Linear Subsidence Rates With Uncertainties for Kabul, Ghazni, Helmand, Farah, Baghlan, Kunduz Provinces

Biennial subsidence rate [cm/y]	Kabul	±	Ghazni	±	Helmand	±	Farah	±	Baghlan	±	Kunduz	±
2014–2015			0.3	0.9	3.6	1.3	0.2	1.7				
2016–2017	5.0	0.7	3.6	0.2	5.5	0.4	4.8	0.5	8.4	1.3	9.9	0.9
2018–2019	6.8	0.5	9.7	0.5	11.3	0.3	4.5	0.5	5.9	0.4	9.2	0.5
2020–2022	3.4	0.4	23.6	0.4	14.3	0.3	6.3	0.3	6.7	0.2		

Note. All units are cm/yr and only significant rates are shown.

5.1. Caveats of InSAR Subsidence Rate Estimates

The impact of the non-closure phase (Ansari et al., 2021; Zheng et al., 2022) on the InSAR subsidence signal in Ghazni (blue square in Figure 7a) does not significantly change the average (linear) rate estimates. With a dense interferometric network (4 neighboring nodes and up to 48 days plus some longer, 1-year connections), we reduced the non-closure phase contribution to ∼3 mm (Text S2 and Figure S2 in Supporting Information S1) (Maghsoudi et al., 2022).

Our visual evaluation of potential contributions from undetected unwrapping errors (Chen & Zebker, 2002) was based on a chain of 13 interferograms exhibiting 26.3 cm of subsidence at the highest subsidence region in the Deh Yak district (Ghazni) in the year of 2021 (Text S3 and Figure S3 in Supporting Information S1). Each interferogram covers a period of 24 days with a quality high enough to exclude unwrapping errors. The fringe density (vertical displacement) reaches a maximum between May and September, which agrees well with the accelerated subsidence during this period of the year observed in the full InSAR time-series (Figure 8b).

5.2. Spatiotemporal Analysis of Afghan Ground Subsidence

To assess whether the subsiding Afghan regions Kabul, Ghazni, Helmand, Farah, Baghlan, Kunduz (Figure 4b) exhibit acceleration over the years, we estimated biennial subsidence rates at the location of maximum subsidence at each region (Table 1, Figure S4 and Text S4 in Supporting Information S1), using a linear regression and the uncertainty derived from the RMS of the residuals. We find accelerated subsidence in Ghazni (∼fivefold in 2018, ∼tenfold in 2021) and in Helmand (∼twofold in 2018), while in Kabul, subsidence halved after 2020. In the other provinces, subsidence rate changes are insignificant.

Subsidence rates in northern Afghanistan (Kunduz and Baghlan) are overall lower than in the southern agricultural regions (Helmand and Ghazni) that rely on groundwater pumping to sustain agriculture. The decelerated subsidence in Kabul correlates with the political regime change in 2020, when almost all of the government, military, and industrial facilities were shut down for a few months, leading to reduced water usage. An alternative water source for the city, such as groundwater recharge interventions using natural surface water, could help reduce the subsidence trend. Additionally, soil layer compaction might decelerate ground subsidence rates once the aquifers are drained.

5.3. Precipitation, Subsidence, and Groundwater Levels in Kabul City

Daqiq et al. (2023) reported 2.6 cm/yr of InSAR subsidence between 2015 and 2017 and 15.1 cm/yr between 2018 and 2020 for Kabul City. Meldebekova et al. (2020) reported 5.3 cm/yr of InSAR subsidence between 2014 and 2019. These numbers agree with our subsidence rate estimate of 5.2 ± 0.6 cm/yr between 2015 and 2019 and confirm the accelerated drop of groundwater levels for Kabul city over the past few years due to the excessive water demand by local population, industries, and institutions (Meldebekova et al., 2020).

The wells with the most significant water-level drop are located at the border of the Kabul basin, where the effect of diminishing groundwater reserves is expected to be highest (Figure 5) (Daqiq et al., 2023; Meldebekova et al., 2020). Peripheral wells usually have the highest water table but also a reduced water-storage capacity and, hence, these wells experience the fastest water-level drops (Zaryab et al., 2022): as groundwater flows toward the center of the basin and water access must be ensured even during dry periods, peripheral

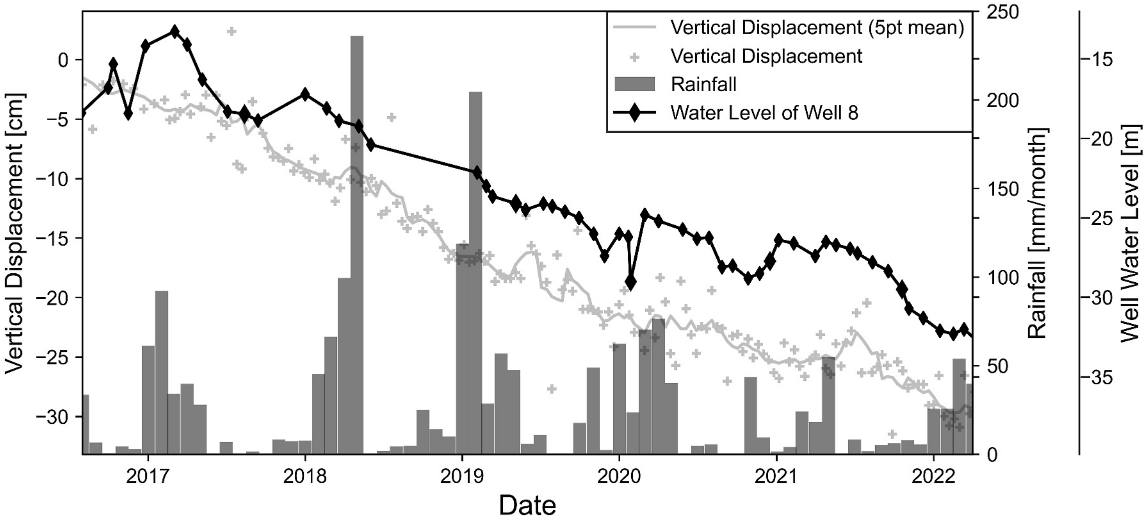

Figure 9. Water level time-series of well 8 (cf. Figure 4 for location), InSAR-based vertical subsidence at the same location, and monthly precipitation. The gray, solid line marks a five-point running mean.

wells must be deeper than central wells (Pauloo et al., 2020). Peripheral wells are often also nearest to the aquifer recharge region (mountains) (Zaryab et al., 2022). The weaker subsidence signal at the outskirts of Kabul might be related to a lower thickness of the conglomeratic layer and talus geology with lower compaction volume (Houben et al., 2009). The lower water level drop in wells near Kabul River and Logar River (Figure 5) might be explained by continuous groundwater recharge by river water, thus stabilizing or partially replenishing the reservoirs during wet seasons (Mahdawi et al., 2022). Seasonal precipitation also mitigates the water table drop and InSAR subsidence (Figure 9). During the rainy winter season (November to March), the water table and water level of wells slightly increase, and subsidence is reduced; during the dry and hot summer season, the water table drops and subsidence accelerates. This periodicity of the water table drop appears to be irreversible; over our observation period, the water table and ground subsidence never compensate, indicating insufficient aquifer net-recharge and, thus, an unsustainable water cycle. The strength of the cyclic signal varies across Kabul city (Figure S5 in Supporting Information S1). Regions with shallow wells (Figure 6f) respond stronger to this cyclic behavior than regions with deep wells (Figure 6d), indicating that surface water only reaches the shallow aquifers. Potential reasons for the overall unsustainable groundwater depletion are increasing temperatures of up to 1.8 C° between 1950 and 2010 (Aich et al., 2017), early snow melting, extended droughts, for example, in 2020 and 2021 (Figure 9), and overpopulation, all causing increased water demand. Water-table drop compels owners to drill deeper wells, leading to economic losses and societal conflicts (pers. comm. Kabul resident Matiullah Kakar).

In addition to the monthly precipitation data, and considering the lack of in-situ discharge data, methods outlined by Jaramillo et al. (2024), along with remote sensing derived or in-situ soil moisture (Zech et al., 2021), could improve the outlook; however, challenges persist due to their limited temporal resolution, coverage, and availability.

5.4. Precipitation, Subsidence, and Groundwater Level in Agricultural Ghazni

Droughts and an increased food demand for agricultural products play a key role in excessive groundwater extraction (Ghobadi-Far et al., 2023). In Ghazni, the droughts in 2020 and 2021 (Figure 10) and the installation of deep irrigation wells (Figure 8a) have led to the depletion of the Kariz networks. Kariz networks are designed to collect and transport shallow groundwater via horizontal, subterranean channels (Figures 7b and 8a). Each channel begins at higher grounds at 40–50 m depth, runs parallel to the steepest surface slope, connects wells at 20–40 m distance, and ends at 2–3 m deep outlets (pers. comm. Deh Yak community leader Alam Khan) (Figure 8a). The number of interconnected wells varies based on the specific location and water demand. The recently installed, solar-powered pumps facilitate access to deeper aquifers at 65–70 m. The spatial

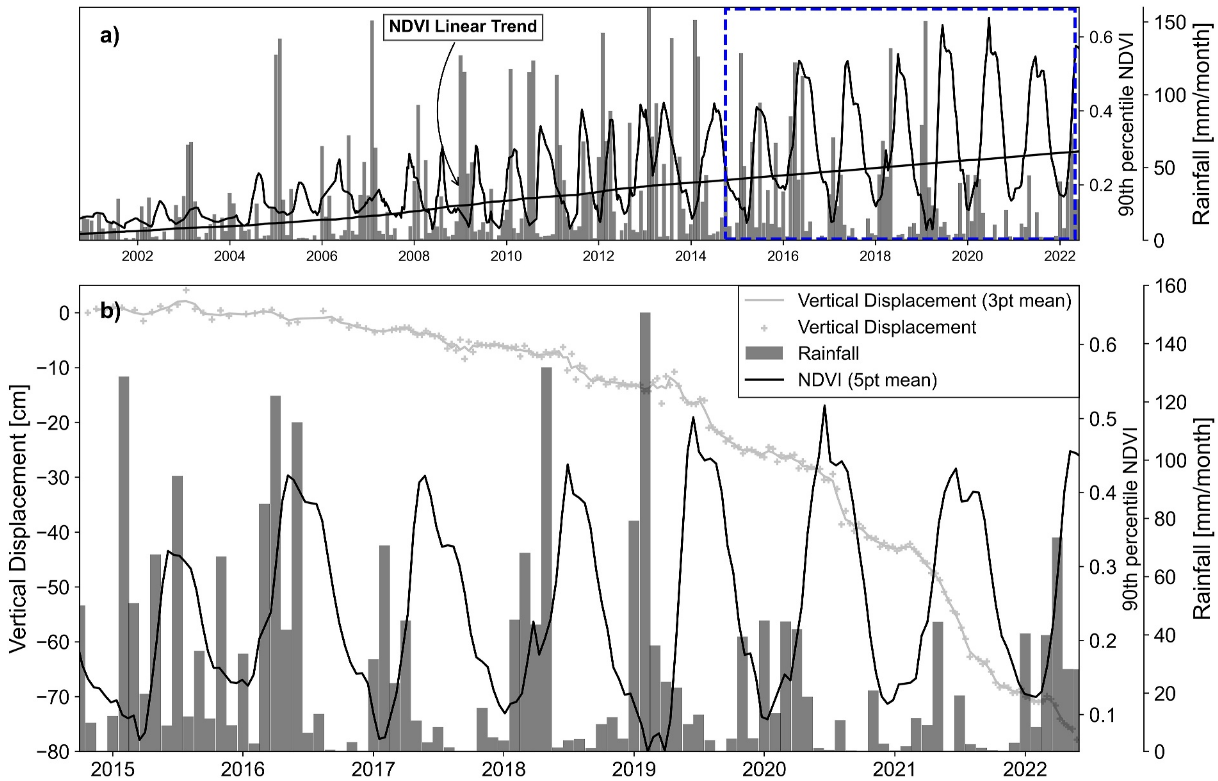

Figure 10. (a) Averaged and seasonal NDVI (Landsat 5 and 8, in black) and precipitation time series (in gray) at the location of maximum subsidence in Deh Yak (blue square in Figure 7a). Blue-dashed area marks the enlargement shown in (b). The NDVI is averaged using a moving window with a length of 5-time steps (about 75 days). (b) As (a) but including vertical displacement InSAR time-series resulting in 77.8 ± 0.5 cm displacement over 7 years.

correlation between the InSAR subsidence pattern and the electric well pumps is higher than the Kariz network (Figure 8a). We, therefore, argue that the subsidence is caused by an increased use of deep irrigation wells leading to aquifer depletion.

Wells are a precondition to reclaim barren land and transforming it into irrigated, arable fields. Comparable subsidence rates have been reported in similar climatic conditions and where excessive groundwater pumping is used to support agricultural practices, for example, in Mashhad, Iran (Naghibi et al., 2022) and in the San Joaquin Valley, California (Jeanne et al., 2019). As a measure for farming intensity, we used NDVI (Figure 10a and 10b) time-series that provides the normalized ratio between the red and near-infrared bands of Landsat 5 and 8 satellite imagery, ranging from 0 (no vegetation) to 1 (abundant vegetation). In our study area, the NDVI varies from ~0.1 in winter to ~0.6 in summer. The high NDVI stands mark periods of high vegetation during dry seasons, indicating groundwater irrigation and the conversion from barren lands to irrigated agriculture lands (Figure 11). Since 2005, the seasonal NDVI variations increased (Figure 10a), gradual at first, but with a significant step in 2016, when solar panel installation began (Figures 7a and 11). Variations in the annual precipitation or the drought years 2020 and 2021 did not affect the NDVI, which suggest plant growth sustained by groundwater irrigation.

Similar to Kabul, we observe irreversible, accelerated ground subsidence during the dry summer season and decelerated subsidence during the wet winter season (Figure 10b), indicating that groundwater recharge from precipitation slightly decelerates subsidence (Murray & Lohman, 2018). In addition, we observe a dramatic acceleration of subsidence over the past 7 years in Ghazni (Figure 10b and Figure S4 in Supporting Information S1). The increase of solar-panel density between 2016 and 2019 by 660% (Figures 8a and 11) is much higher than in southern Afghanistan (Helmand and Kandahar), where the number of solar panels increased by 80% during 2016 and 2017 (Mansfield, 2019).

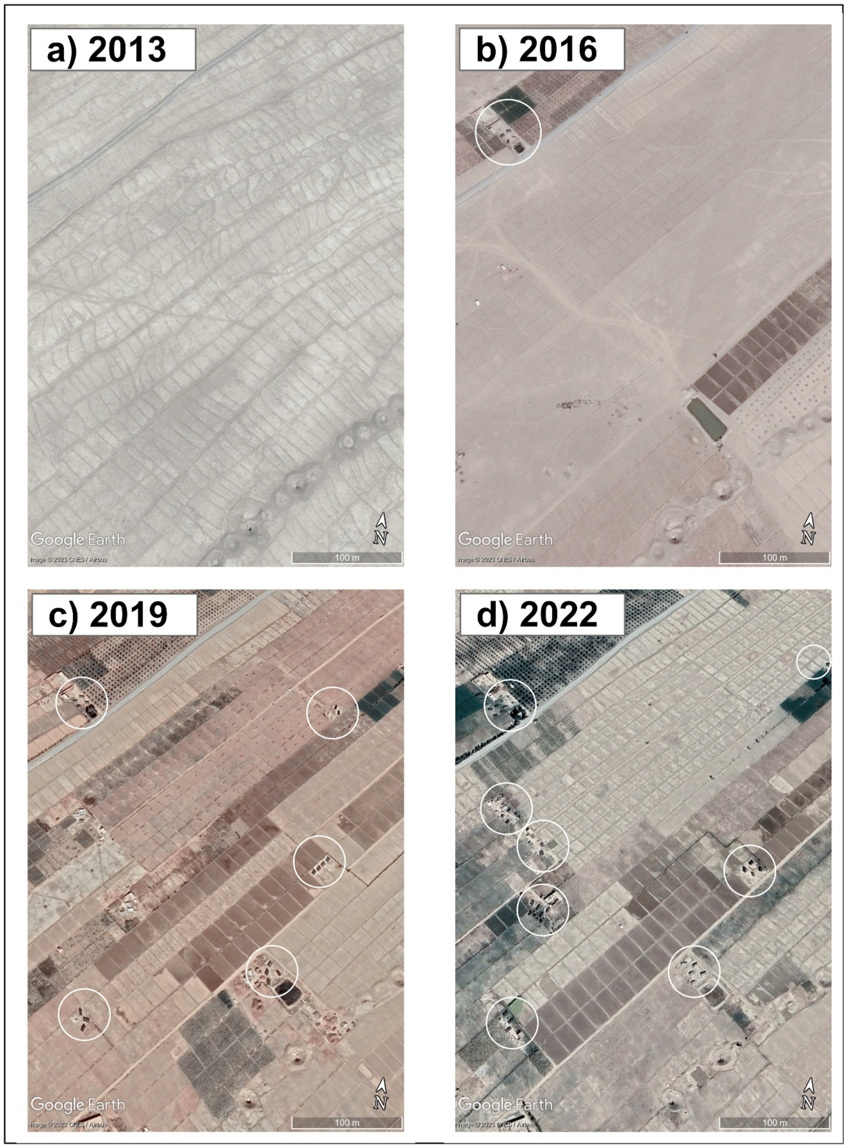

Figure 11. Mapped solar panel arrays (white circles) on historical GoogleEarth Pro optical imagery of Deh Yak acquired in (a–d) 2013, 2016, 2019, and 2022. The arrays are essential to pump ground water and turn barren or rainfed land into agricultural land.

Subsidence strongly accelerated after 2019 and ∼3 years after the beginning of deep-well pump installations. The drought years 2020 and 2021 probably intensified this process, causing a km-long desiccation crack at the surface (Figure 7b). Such cracks were also reported in Yazd, Iran, after excessive water extraction for irrigation (Amin et al., 2019).

6. Conclusions

Countrywide InSAR rate maps from 2015 to 2022 highlight for the first time several significantly subsiding regions in northern (Baghlan, Kunduz) and southern Afghanistan (Farah, Helmand, Ghazni, Kabul). Vertical subsidence rates in Helmand are 6.4 ± 0.2 cm/yr between 2015 and early-2018 and 13.9 ± 0.1 cm/yr between mid-2018 and 2022, in Farah 5.1 ± 0.1 cm/yr, in Baghlan 6.6 ± 0.1 cm/yr, and in Kunduz 8.9 ± 0.2 cm/yr. We observe that urban subsidence rates are relatively stable, but some rural and intensely farmed environments show accelerated subsidence.

In Kabul city, we observed a maximum subsidence rate of 5.1 ± 0.1 cm/yr (31.2 ± 0.5 cm in total for 6 years). We attribute this to increased groundwater exploitation due to the rapid growth of population and industry. Shallow, peripheral wells located at the edge of the sedimentary basin experience a higher water-level drop than central wells. Over our observation period, the water-table drop slightly recovers each year by seasonal precipitation, but both, subsidence and water-table drop, continue irreversibly.

Subsidence in the irrigation-fed agricultural areas of Deh Yak, Ghazni, dramatically accelerated: In mid-2018 the subsidence rates increased five times and in 2021 10 times compared to the subsidence rates measured before mid-2018. The acceleration is spatiotemporally linked with the increase of electrical water pumps, which we identified by mapping solar-panel arrays, and the reduction in using traditional Kariz systems. In the past decade, a large amount of barren land was transformed into agricultural land caused by access to groundwater. We measured a maximum of 77.8 ± 0.5 cm subsidence over 7 years in this area, causing m-wide and km-long desiccation cracks.

Our study highlights the vast extent of unsustainable groundwater use affecting almost all larger cities and agricultural centers in Afghanistan. Similar processes are reported not only from countries with similar socio-economic, agricultural, and climatic conditions like Iran (e.g., Naghibi et al., 2022), but also from developed countries like the United States of America (e.g., Jeanne et al., 2019), Spain (e.g., Papadaki, 2014), and Greece (e.g., Mateos et al., 2017). The affected regions are often located in sedimentary basins with unconsolidated units and high permeability. For future studies we propose to classify the spatiotemporal behavior of the subsidence to better discriminate when, where, and how subsidence is coupled with water table recovery. In turn, this will help to take precise actions to mitigate permanent water loss.

Data Availability Statement

This work contains modified open access Copernicus Sentinel-1 data produced by COMET LiCSAR service (Lazecký et al., 2020) processed with LiCSBAS (Morishita et al., 2020) and MintPy (Yunjun et al., 2019). Background map data are provided by Google Earth Engine (Google Earth Engine, 2024). High-resolution optical imagery is provided by Maxar (Maxar Technologies, 2023) and accessed through ArcGIS online services (Esri, 2024) hosted by Esri and Google Earth Pro (Google LLC, 2024). Precipitation time-series, NDVI time-series, Kabul well logs, high-resolution subsidence rate maps, shapefiles, and Jupyter notebook to produce key figures are available at Kakar et al. (2024).

Acknowledgments

Dr. Manudeo Singh advised us on the use of MintPy. Matiullah Kakar provided insights into the current socio-economic conditions in Kabul. The Norwegian Afghanistan Committee (afghanistan.no) arranged and supported field visits in Ghazni. This research was conducted under the Green Central Asia Initiative grant (AA7090002) provided by the German Ministry of Foreign Affairs. Open Access funding enabled and organized by Projekt DEAL.

References

Abdullah, S. H., Chmyriov, V. M., & Dronov, V. I. (2008). *Geology and mineral resources of Afghanistan (Vol. 15)*. British Geological Survey Occasional Publication. Retrieved from https://nora.nerc.ac.uk/id/eprint/3723

Aich, V., Akhundzadah, N., Knuerr, A., Khoshbeen, A., Hattermann, F., Paeth, H., et al. (2017). Climate change in Afghanistan Deduced from Reanalysis and Coordinated regional climate Downscaling Experiment (CORDEX)—South Asia simulations. *Climate*, *5*(2), 38. https://doi.org/10.3390/cli5020038

Amin, P., Ghalibaf, M. A., & Hosseini, M. (2019). Land subsidence and soil cracks monitoring by surveying on the clayey plain soils in Central Iran (case study: Yazd City). *Arabian Journal of Geosciences*, *12*(3), 84. https://doi.org/10.1007/s12517-019-4241-3

Ansari, H., De Zan, F., & Parizzi, A. (2021). Study of systematic bias in measuring surface deformation with SAR interferometry. *IEEE Transactions on Geoscience and Remote Sensing*, *59*(2), 1285–1301. https://doi.org/10.1109/TGRS.2020.3003421

Bell, J. W., Amelung, F., Ramelli, A. R., & Blewitt, G. (2002). Land subsidence in Las Vegas, Nevada, 1935-2000: New geodetic data show evolution, revised spatial patterns, and reduced rates. *Environmental and Engineering Geoscience*, *8*(3), 155–174. https://doi.org/10.2113/8.3.155

Berardino, P., Fornaro, G., Lanari, R., & Sansosti, E. (2002). A new algorithm for surface deformation monitoring based on small baseline differential SAR interferograms. *IEEE Transactions on Geoscience and Remote Sensing*, *40*(11), 2375–2383. https://doi.org/10.1109/TGRS.2002.803792

Biggs, J., Wright, T., Lu, Z., & Parsons, B. (2007). Multi-interferogram method for measuring interseismic deformation: Denali Fault, Alaska. *Geophysical Journal International*, *170*(3), 1165–1179. https://doi.org/10.1111/j.1365-246X.2007.03415.x

Bitelli, G. (1991). Levelling data management for the monitoring of land subsidence. *Proceedings of the Fourth International Symposium on Land Subsidence. Houston, TX, USA*, *1*, 12–17.

Boergens, E., Kvas, A., Eicker, A., Dobslaw, H., Schawohl, L., Dahle, C., et al. (2022). Uncertainties of GRACE-based terrestrial water storage anomalies for arbitrary averaging regions. *Journal of Geophysical Research: Solid Earth*, *127*(2). https://doi.org/10.1029/2021JB022081

Bott, L.-M., Schöne, T., Illigner, J., Haghshenas Haghighi, M., Gisevius, K., & Braun, B. (2021). Land subsidence in Jakarta and Semarang Bay – The relationship between physical processes, risk perception, and household adaptation. *Ocean & Coastal Management*, *211*, 105775. https://doi.org/10.1016/j.ocecoaman.2021.105775

Chaussard, E., Havazli, E., Fattahi, H., Cabral-Cano, E., & Solano-Rojas, D. (2021). Over a century of sinking in Mexico City: No hope for significant elevation and storage capacity recovery. *Journal of Geophysical Research: Solid Earth*, *126*(4), e2020JB020648. https://doi.org/10.1029/2020JB020648

Chen, C. W., & Zebker, H. A. (2002). Phase unwrapping for large SAR interferograms: Statistical segmentation and generalized network models. *IEEE Transactions on Geoscience and Remote Sensing*, *40*(8), 1709–1719. https://doi.org/10.1109/TGRS.2002.802453

Daqiq, M. T., Sharma, R., Karunakalage, A., & Kannaujiya, S. (2023). Determination of groundwater storage variation, deficit, and abstraction in Afghanistan and the assessment of the evolution of vadose zone in Kabul City. *IEEE Transactions on Geoscience and Remote Sensing*, *61*, 1–18. https://doi.org/10.1109/TGRS.2023.3326164

De Zan, F., Zonno, M., & Lopez-Dekker, P. (2015). Phase inconsistencies and multiple scattering in SAR interferometry. *IEEE Transactions on Geoscience and Remote Sensing*, *53*(12), 6608–6616. https://doi.org/10.1109/TGRS.2015.2444431

Ebrahimi, A., Mehraban, Y., Omidvarborna, H., Vakilinejad, A., & Al-Sayigh, A. R. S. (2021). Kariz (ancient aqueduct) system: A review on geoengineering and environmental studies. *Environmental Earth Sciences*, *80*(6), 236. https://doi.org/10.1007/s12665-021-09545-2

Eqbal, S. (2022). *One-kilometer-long surface fault occurs in Central Afghanistan*. Khaama Press. Retrieved from https://www.khaama.com/one-kilometer-long-surface-fault-occurs-in-central-afghanistan-47483/

Esri. (2024). ArcGIS desktop (version 10.8.2). *Software*. Retrieved from https://www.esri.com/en-us/arcgis/products/arcgis-desktop

FAO. (2021). Aggregated land cover database of the Islamic Republic of Afghanistan (2010). *Dataset*. Retrieved from https://data.apps.fao.org/map/catalog/srv/api/records/1dd35e22-bd51-4c4d-bf0c-546baababe74

Farr, T. G., & Kobrick, M. (2000). Shuttle radar topography mission produces a wealth of data. *Eos, Transactions American Geophysical Union*, *81*(48), 583–585. https://doi.org/10.1029/EO081i048p00583

Fattahi, H., & Amelung, F. (2013). DEM error correction in InSAR time series. *Geoscience and Remote Sensing, IEEE Transactions On*, *51*(7), 4249–4259. https://doi.org/10.1109/TGRS.2012.2227761

Fernández-Torres, E., Cabral-Cano, E., Solano-Rojas, D., Havazli, E., & Salazar-Tlaczani, L. (2020). Land subsidence risk maps and InSAR based angular distortion structural vulnerability assessment: An example in Mexico city. *Proceedings of the International Association of Hydrological Sciences*, *382*, 583–587. https://doi.org/10.5194/piahs-382-583-2020

Ferretti, A., Prati, C., & Rocca, F. (2001). Permanent scatterers in SAR interferometry. *IEEE Transactions on Geoscience and Remote Sensing*, *39*(1), 8–20. https://doi.org/10.1109/36.898661

Flechtner, F., Neumayer, K.-H., Dahle, C., Dobslaw, H., Fagiolini, E., Raimondo, J.-C., & Güntner, A. (2016). What can be expected from the GRACE-FO laser ranging interferometer for Earth Science applications? *Space Sciences Series of ISSI*, 263–280. https://doi.org/10.1007/978-3-319-32449-4_11

Floris, M., Fontana, A., Tessari, G., & Mulè, M. (2019). Subsidence zonation through satellite interferometry in coastal plain environments of NE Italy: A possible tool for geological and geomorphological mapping in urban areas. *Remote Sensing*, *11*(2), 165. https://doi.org/10.3390/rs11020165

Froese, C. R., & Shilong, M. (2008). Mapping and monitoring coal mine subsidence using LiDAR and InSAR. *GeoEdmonton*, *8*, 1127–1133.

Ghobadi-Far, K., Werth, S., Shirzaei, M., & Bürgmann, R. (2023). Spatiotemporal groundwater storage dynamics and aquifer mechanical properties in the Santa Clara valley inferred from InSAR deformation over 2017–2022. *Geophysical Research Letters*, *50*(22). https://doi.org/10.1029/2023GL105157

Goldstein, R. M., & Werner, C. L. (1998). Radar interferogram filtering for geophysical applications. *Geophysical Research Letters*, *25*(21), 4035–4038. https://doi.org/10.1029/1998GL900033

Google Earth Engine. (2024). Google Earth Engine: A global platform for environmental data analysis. *Dataset*. Retrieved from https://earthengine.google.com

Google LLC. (2024). Google Earth Pro. *Software*. Retrieved from https://www.google.com/earth/versions

Green, T. R., Taniguchi, M., Kooi, H., Gurdak, J. J., Allen, D. M., Hiscock, K. M., et al. (2011). Beneath the surface of global change: Impacts of climate change on groundwater. *Journal of Hydrology*, *405*(3–4), 532–560. https://doi.org/10.1016/j.jhydrol.2011.05.002

Haghshenas Haghighi, M., & Motagh, M. (2019). Ground surface response to continuous compaction of aquifer system in Tehran, Iran: Results from a long-term multi-sensor InSAR analysis. *Remote Sensing of Environment*, *221*, 534–550. https://doi.org/10.1016/j.rse.2018.11.003

Haghshenas Haghighi, M., & Motagh, M. (2024). Uncovering the impacts of depleting aquifers: A remote sensing analysis of land subsidence in Iran. *Science Advances*, *10*(19). https://doi.org/10.1126/sciadv.adk3039

Hamidi, M. D., Kissane, S., Bogush, A. A., Karim, A. Q., Sagintayev, J., Towers, S., & Greenwell, H. C. (2023). Spatial estimation of groundwater quality, hydrogeochemical investigation, and health impacts of shallow groundwater in Kabul city, Afghanistan. *Sustainable Water Resources Management*, *9*(1), 20. https://doi.org/10.1007/s40899-022-00808-9

Hekmat, H., Ahmad, T., Singh, S. K., Kanga, S., Meraj, G., & Kumar, P. (2023). Land use and land cover changes in Kabul, Afghanistan focusing on the Drivers impacting urban dynamics during five decades 1973–2020. *Geomatics*, *3*(3), 447–464. https://doi.org/10.3390/geomatics3030024

Herrera-García, G., Ezquerro, P., Tomás, R., Béjar-Pizarro, M., López-Vinielles, J., Rossi, M., et al. (2021). Mapping the global threat of land subsidence. *Science*, *371*(6524), 34–36. https://doi.org/10.1126/science.abb8549

Homilius, J. (1966). Hydrogeologische und geoelektrische Untersuchungen in den Kabul-Becken, Afghanistan; Teil 2: Geoelektrischer Bericht 1965/66 [Hydrogeological and geoelectrical investigations in the Kabul Basin, Afghanistan, Part 2: Report on geoelectrics 1965/66]. BGR file number 0020506. BRG.

Houben, G., Niard, N., Tünnermeier, T., & Himmelsbach, T. (2009). Hydrogeology of the Kabul basin (Afghanistan), part I: Aquifers and hydrology. *Hydrogeology Journal*, *17*(3), 665–677. https://doi.org/10.1007/s10040-008-0377-z

Huffman, G. J., Stocker, E. F., Bolvin, D. T., Nelkin, E. J., & Jackson, T. (2023). GPM IMERG final precipitation L3 half hourly 0.1 degree x 0.1 degree V06, [Dataset]. *Goddard Earth Sciences Data and Information Services Center (GES DISC)*. https://doi.org/10.5067/GPM/IMERG/3B-MONTH/06

Ikehara, M. E. (1994). Global positioning system surveying to monitor land subsidence in Sacramento valley, California, USA. *Hydrological Sciences Journal*, *39*(5), 417–429. https://doi.org/10.1080/02626669409492765

Jaramillo, F., Aminjafari, S., Castellazzi, P., Fleischmann, A., Fluet-Chouinard, E., Hashemi, H., et al. (2024). The potential of Hydrogeodesy to Address water-related and Sustainability challenges. *Water Resources Research*, *60*(11). https://doi.org/10.1029/2023WR037020

Jeanne, P., Farr, T. G., Rutqvist, J., & Vasco, D. W. (2019). Role of agricultural activity on land subsidence in the San Joaquin Valley, California. *Journal of Hydrology*, *569*, 462–469. https://doi.org/10.1016/j.jhydrol.2018.11.077

Jolivet, R., Agram, P. S., Lin, N. Y., Simons, M., Doin, M., Peltzer, G., & Li, Z. (2014). Improving InSAR geodesy using global atmospheric models. *Journal of Geophysical Research: Solid Earth*, *119*(3), 2324–2341. https://doi.org/10.1002/2013JB010588

Kakar, N., Metzger, S., Schöne, T., Motagh, M., Waizy, H., Nasrat, N. A., et al. (2024). High-resolution subsidence maps and data for whole Afghanistan, and, in a higher resolution, for Kabul and Ghazni provinces (2015-2022) [Dataset]. *GFZ Data Services*. https://doi.org/10.5880/GFZ.1.2.2024.001

Karim, A. Q., & Sadat, S. H. (2021). Groundwater of Afghanistan (potential capacity, scarcity, security issues, and solutions). In *Global groundwater* (pp. 323–328). https://doi.org/10.1016/B978-0-12-818172-0.00023-2

Kennedy, J. H., Kristenson, H., Johnston, A., Rine, J., Logan, T., & bot, A. A. team. (2021). ASFHyP3/hyp3-docs: HyP3 docs v0.3.17. https://doi.org/10.5281/zenodo.5542916

Lazecký, M., Spaans, K., González, P. J., Maghsoudi, Y., Morishita, Y., Albino, F., et al. (2020). LiCSAR: An automatic InSAR tool for measuring and monitoring tectonic and volcanic activity. *Remote Sensing*, *12*(15), 2430. https://doi.org/10.3390/rs12152430

Long, D., Chen, X., Scanlon, B. R., Wada, Y., Hong, Y., Singh, V. P., et al. (2016). Have GRACE satellites overestimated groundwater depletion in the Northwest India Aquifer? *Scientific Reports*, *6*(1), 24398. https://doi.org/10.1038/srep24398

López-Quiroz, P., Doin, M.-P., Tupin, F., Briole, P., & Nicolas, J.-M. (2009). Time series analysis of Mexico City subsidence constrained by radar interferometry. *Journal of Applied Geophysics*, *69*(1), 1–15. https://doi.org/10.1016/j.jappgeo.2009.02.006

Mack, T. J., Chornack, M. P., & Taher, M. R. (2013). Groundwater-level trends and implications for sustainable water use in the Kabul Basin, Afghanistan. *Environment Systems and Decisions*, *33*(3), 457–467. https://doi.org/10.1007/s10669-013-9455-4

Macpherson, G. L., Johnson, W. C., & Liu, H. (2017). Viability of karezes (ancient water supply systems in Afghanistan) in a changing world. *Applied Water Science*, *7*(4), 1689–1710. https://doi.org/10.1007/s13201-015-0336-5

Maghsoudi, Y., Hooper, A. J., Wright, T. J., Lazecky, M., & Ansari, H. (2022). Characterizing and correcting phase biases in short-term, multilooked interferograms. *Remote Sensing of Environment*, *275*, 113022. https://doi.org/10.1016/j.rse.2022.113022

Mahdawi, Q., Sagin, J., Absametov, M., & Zaryab, A. (2022). Water recharges suitability in Kabul aquifer system within the upper indus basin. *Water*, *14*(15), 2390. https://doi.org/10.3390/w14152390

Mansfield, D. (2019). On the frontiers of development: Illicit Poppy and the transformation of the deserts of southwest Afghanistan. *Journal of Illicit Economies and Development*, *1*(3), 330–345. https://doi.org/10.31389/jied.46

Massonnet, D., & Feigl, K. L. (1998). Radar interferometry and its application to changes in the Earth's surface. *Reviews of Geophysics*, *36*(4), 441–500. https://doi.org/10.1029/97RG03139

Mateos, R. M., Ezquerro, P., Luque-Espinar, J. A., Béjar-Pizarro, M., Notti, D., Azañón, J. M., et al. (2017). Multiband PSInSAR and long-period monitoring of land subsidence in a strategic detrital aquifer (Vega de Granada, SE Spain): An approach to support management decisions. *Journal of Hydrology*, *553*, 71–87. https://doi.org/10.1016/j.jhydrol.2017.07.056

Maxar Technologies. (2023). WorldView-3 satellite imagery, April 27. *Dataset*. Retrieved from https://www.maxar.com/

Meldebekova, G., Yu, C., Li, Z., & Song, C. (2020). Quantifying ground subsidence associated with aquifer overexploitation using space-borne radar interferometry in Kabul, Afghanistan. *Remote Sensing*, *12*(15), 2461. https://doi.org/10.3390/rs12152461

Morishita, Y., Lazecky, M., Wright, T., Weiss, J., Elliott, J., & Hooper, A. (2020). LiCSBAS: An open-source InSAR time series analysis package integrated with the LiCSAR automated sentinel-1 InSAR processor. *Remote Sensing*, *12*(3), 424. https://doi.org/10.3390/rs12030424

Motagh, M., Djamour, Y., Walter, T. R., Wetzel, H.-U., Zschau, J., & Arabi, S. (2007). Land subsidence in Mashhad valley, northeast Iran: Results from InSAR, levelling and GPS. *Geophysical Journal International*, *168*(2), 518–526. https://doi.org/10.1111/j.1365-246X.2006.03246.x

Motagh, M., Walter, T. R., Sharifi, M. A., Fielding, E., Schenk, A., Anderssohn, J., & Zschau, J. (2008). Land subsidence in Iran caused by widespread water reservoir overexploitation. *Geophysical Research Letters*, *35*(16). https://doi.org/10.1029/2008GL033814

Muradi, A. J., & Boz, I. (2018). The contribution of agriculture sector in the economy of Afghanistan. *International Journal of Scientific Research and Management (IJSRM)*, *6*(10). https://doi.org/10.18535/ijsrm/v6i10.em04

Murray, K. D., & Lohman, R. B. (2018). Short-lived pause in Central California subsidence after heavy winter precipitation of 2017. *Science Advances*, *4*(8). https://doi.org/10.1126/sciadv.aar8144

Naghibi, S. A., Khodaei, B., & Hashemi, H. (2022). An integrated InSAR-machine learning approach for ground deformation rate modeling in arid areas. *Journal of Hydrology*, *608*, 127627. https://doi.org/10.1016/j.jhydrol.2022.127627

National Statistic and Information Authority (NSIA). (2023). Estimated population of Afghanistan 2022-2023. Retrieved from http://nsia.gov.af/

Neely, W. R., Borsa, A. A., Burney, J. A., Levy, M. C., Silverii, F., & Sneed, M. (2021). Characterization of groundwater recharge and flow in California's San Joaquin Valley from InSAR-observed surface deformation. *Water Resources Research*, *57*(4). https://doi.org/10.1029/2020WR028451

NEPA & UN Environment. (2016). *Afghanistan: Climate change science perspectives*. National Environmental Protection Agency & UN Environment. Retrieved from https://www.acbar.org/upload/1493192115761.pdf

Papadaki, E. S. (2014). Monitoring subsidence at Messara basin using radar interferometry. *Environmental Earth Sciences*, *72*(6), 1965–1977. https://doi.org/10.1007/s12665-014-3105-0

Pauloo, R. A., Escriva-Bou, A., Dahlke, H., Fencl, A., Guillon, H., & Fogg, G. E. (2020). Domestic well vulnerability to drought duration and unsustainable groundwater management in California's Central Valley. *Environmental Research Letters*, *15*(4), 044010. https://doi.org/10.1088/1748-9326/ab6f10

Pepe, A., Bonano, M., Zhao, Q., Yang, T., & Wang, H. (2016). The use of C-/X-band time-gapped SAR data and geotechnical models for the study of Shanghai's ocean-reclaimed lands through the SBAS-DInSAR technique. *Remote Sensing*, *8*(11), 911. https://doi.org/10.3390/rs8110911

Perissin, D., & Wang, T. (2012). Repeat-pass SAR interferometry with partially coherent targets. *IEEE Transactions on Geoscience and Remote Sensing*, *50*(1), 271–280. https://doi.org/10.1109/TGRS.2011.2160644

Qutbudin, I., Shiru, M. S., Sharafati, A., Ahmed, K., Al-Ansari, N., Yaseen, Z. M., et al. (2019). Seasonal drought pattern changes due to climate variability: Case study in Afghanistan. *Water*, *11*(5), 1096. https://doi.org/10.3390/w11051096

Ren, H., & Feng, X. (2020). Calculating vertical deformation using a single InSAR pair based on singular value decomposition in mining areas. *International Journal of Applied Earth Observation and Geoinformation*, *92*, 102115. https://doi.org/10.1016/j.jag.2020.102115

Sarwary, M., Senthilnathan, S., Saravanakumar, V., Arivelarasan, T., & Manivasagam, V. S. (2022). Climate risks, farmers perception and adaptation strategies to climate variability in Afghanistan. *Emirates Journal of Food and Agriculture*. https://doi.org/10.9755/ejfa.2021.v33.i12.2797

Schmidt, D. A., & Bürgmann, R. (2003). Time-dependent land uplift and subsidence in the Santa Clara valley, California, from a large interferometric synthetic aperture radar data set. *Journal of Geophysical Research*, *108*(B9). https://doi.org/10.1029/2002JB002267

Shokory, J. A. N., Schaefli, B., & Lane, S. N. (2023). Water resources of Afghanistan and related hazards under rapid climate warming: A review. *Hydrological Sciences Journal*, *68*(3), 507–525. https://doi.org/10.1080/02626667.2022.2159411

Silverman, B. W. (2018). *Density estimation for statistics and data analysis*. Routledge. https://doi.org/10.1201/9781315140919

Sims, K., Reith, A., Bright, E., McKee, J., & Rose, A. (2021). LandScan global 2021 [dataset]. Oak Ridge National Laboratory. Oak Ridge National Laboratory. https://doi.org/10.48690/1527702

Siriwardane-de Zoysa, R., Schöne, T., Herbeck, J., Illigner, J., Haghighi, M., Simarmata, H., et al. (2021). The 'wickedness' of governing land subsidence: Policy perspectives from urban Southeast Asia. *PLoS One*, *16*(6), e0250208. https://doi.org/10.1371/journal.pone.0250208

Sneed, M., & Brandt, J. T. (2015). Land subsidence in the san Joaquin Valley, California, USA, 2007–2014. *Proceedings of the International Association of Hydrological Sciences*, *372*, 23–27. https://doi.org/10.5194/piahs-372-23-2015

Torres, R., Snoeij, P., Geudtner, D., Bibby, D., Davidson, M., Attema, E., et al. (2012). GMES Sentinel-1 mission. *Remote Sensing of Environment*, *120*, 9–24. https://doi.org/10.1016/j.rse.2011.05.028

Yu, C., Li, Z., Penna, N. T., & Crippa, P. (2018). Generic atmospheric correction model for interferometric synthetic aperture radar observations. *Journal of Geophysical Research: Solid Earth*, *123*(10), 9202–9222. https://doi.org/10.1029/2017JB015305

Yunjun, Z., Fattahi, H., & Amelung, F. (2019). Small baseline InSAR time series analysis: Unwrapping error correction and noise reduction. *Computers & Geosciences*, *133*, 104331. https://doi.org/10.1016/j.cageo.2019.104331

Zaryab, A., Nassery, H. R., & Alijani, F. (2022). The effects of urbanization on the groundwater system of the Kabul shallow aquifers, Afghanistan. *Hydrogeology Journal*, *30*(2), 429–443. https://doi.org/10.1007/s10040-021-02445-6

Zech, C., Schöne, T., Illigner, J., Stolarczuk, N., Queißer, T., Köppl, M., et al. (2021). Hydrometeorological data from a remotely operated multi-parameter station network in Central Asia. *Earth System Science Data*, *13*(3), 1289–1306. https://doi.org/10.5194/essd-13-1289-2021

Zheng, Y., Fattahi, H., Agram, P., Simons, M., & Rosen, P. (2022). On closure phase and systematic bias in multilooked SAR interferometry. *IEEE Transactions on Geoscience and Remote Sensing*, *60*, 1–11. https://doi.org/10.1109/TGRS.2022.3167648

References From the Supporting Information

Kübler, S., Rucina, S., Aßbichler, D., Eckmeier, E., & King, G. (2021). Lithological and topographic impact on soil nutrient distributions in tectonic landscapes: Implications for pleistocene human-landscape interactions in the southern Kenya rift. *Frontiers in Earth Science*, *9*. https://doi.org/10.3389/feart.2021.611687